

# Organophosphonate-Based PNA-Functionalization of Silicon Nanowires for Label-Free DNA Detection

Anna Cattani-Scholz,<sup>†</sup> Daniel Pedone,<sup>†</sup> Manish Dubey,<sup>‡</sup> Stefan Neppi,<sup>§</sup> Bert Nickel,<sup>⊥</sup> Peter Feulner,<sup>§</sup> Jeffrey Schwartz,<sup>‡</sup> Gerhard Abstreiter,<sup>†</sup> and Marc Tornow<sup>||,\*</sup>

<sup>†</sup>Walter Schottky Institute, Technical University Munich, Am Coulombwall, 85748 Germany, <sup>‡</sup>Department of Chemistry, Princeton University, Princeton, New Jersey 08544, <sup>§</sup>Department of Physics, Technical University Munich, James Franck Strasse, 85748 Garching, Germany, <sup>⊥</sup>Ludwig-Maximilian University Munich, Geschwister-Scholl-Platz 1, 80539 Munich, Germany, and <sup>||</sup>Institute of Semiconductor Technology, Technical University Braunschweig, Hans-Sommer-Strasse 66, 38106 Braunschweig, Germany

Silicon-based field effect devices have been widely investigated in recent years for the label-free detection of DNA hybridization. These devices span a broad range of geometries including planar sensor structures with capacitive readout,<sup>1</sup> electrolyte-gated field-effect transistor (ISFET) devices,<sup>2,3</sup> arrays,<sup>4</sup> and silicon nanowires prepared by various techniques.<sup>5–7</sup> Among the many different semiconductor materials that have been studied for biosensor applications, silicon provides a good compromise between stability, biocompatibility, and maturity of the semiconductor processing technology.<sup>8</sup> The devices rely on detecting changes in the electrical surface potential that occur as a result of adsorbing charged DNA. This signal transduction mechanism is free from the need to modify the target DNA molecules by, for example, fluorescent dyes; hence it constitutes a label-free detection method. To provide surface-immobilized affinity receptors for DNA hybridization, a suitable organic interface is obligatory that has a high density of receptor binding sites and a short linker distance between surface and probe DNA or its analogue, peptidic nucleic acid (PNA), to minimize electrolyte screening effects.<sup>9,10</sup> Well-known approaches for direct attachment of DNA to the natural silicon oxide surface either involve tethering it nonspecifically to a positively charged poly-L-lysine layer on the surface, or covalently binding it to an end-functionalized siloxane layer that is grafted onto the silicon oxide surface. Several shortcomings of siloxane interfaces for the controlled, covalent attachment of DNA to silicon oxide surfaces include limited

**ABSTRACT** We investigated hydroxyalkylphosphonate monolayers as a novel platform for the biofunctionalization of silicon-based field effect sensor devices. This included a detailed study of the thin film properties of organophosphonate films on Si substrates using several surface analysis techniques, including AFM, ellipsometry, contact angle, X-ray photoelectron spectroscopy (XPS), X-ray reflectivity, and current–voltage characteristics in electrolyte solution. Our results indicate the formation of a dense monolayer on the native silicon oxide that has excellent passivation properties. The monolayer was biofunctionalized with 12 mer peptide nucleic acid (PNA) receptor molecules in a two-step procedure using the heterobifunctional linker, 3-maleimidopropionic acid-*N*-hydroxysuccinimide ester. Successful surface modification with the probe PNA was verified by XPS and contact angle measurements, and hybridization with DNA was determined by fluorescence measurements. Finally, the PNA functionalization protocol was translated to 2  $\mu\text{m}$  long, 100 nm wide Si nanowire field effect devices, which were successfully used for label-free DNA/PNA hybridization detection.

**KEYWORDS:** biosensor · DNA/PNA hybridization · surface characterization · XPS · X-ray reflectivity · organophosphonate monolayers · heterobifunctional linker · silicon nanowire device

hydrolytic stability, critical dependence on available hydroxyl binding sites on the  $\text{SiO}_2$ , and the intrinsic risk of multilayer formation; few reports of alternative interfaces have appeared. A desirable interface should promote surface receptor conformational control with high target molecule binding efficiency through good accessibility to the binding sites. Here, an organized, covalently bound interface should be superior to nonspecific systems that rely simply on physisorption. Self-assembled monolayers of organophosphonates provide one such platform; they are stable and elegant systems that can be used to bond biological systems to native silicon oxide surfaces and thus obviate many disadvantages of siloxane interfaces.<sup>11,12</sup>

In this article we describe the biofunctionalization of silicon oxide-terminated surfaces with PNA<sup>13</sup> oligonucleotides,

\*Address correspondence to m.tornow@tu-bs.de.

Received for review March 6, 2008 and accepted June 25, 2008.

10.1021/nn800136e CCC: \$40.75

© XXXX American Chemical Society

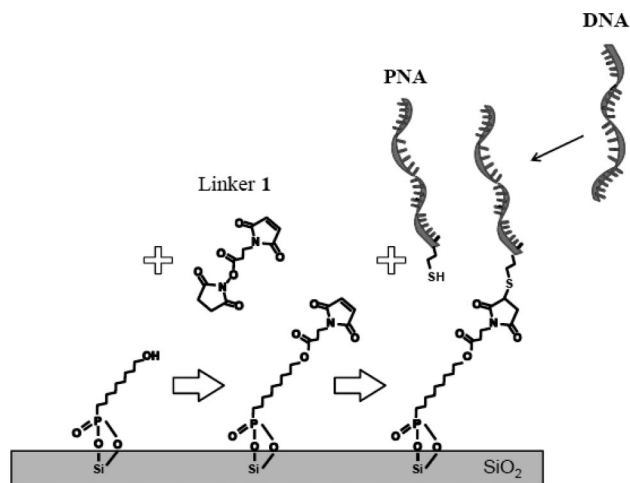


**Figure 1.** Schematic illustration of the stepwise functionalization of the SiO<sub>2</sub>-terminated Si surface. PNA is coupled to a monolayer of 11-hydroxyundecylphosphonate using the heterobifunctional linker, 3-maleimidopropionic-acid-*N*-hydroxysuccinimide, **1**. Following attachment via the maleimido moiety, single stranded PNA serves as a receptor for hybridization with target DNA.

which are receptors for DNA hybridization, using alkylphosphonate monolayers. In contrast to DNA, PNA does not have an anionic phosphate backbone, and is therefore uncharged at neutral pH.<sup>14</sup> The lack of repulsion between PNA and DNA results in enhanced hybridization efficiency and increased melting temperature, which is almost independent from the salt concentration of the medium. Moreover, the expected increase in net charge before and after hybridization of the DNA/PNA system exceeds the one of DNA/DNA.<sup>15</sup> Taking these two features together, a larger measurable change in surface potential is to be expected upon hybridization.

As shown in Figure 1, we employed a stepwise functionalization protocol using 11-hydroxyundecylphosphonate and a maleimide heterobifunctional linker system. First, we report the characterization of both the hydroxyl-terminated phosphonate monolayers and the biohybridized thin films that we synthesized on planar substrates. We used several surface analytical methods, including contact angle measurements, ellipsometry, X-ray photoelectron spectroscopy (XPS), X-ray reflectivity, atomic force microscopy (AFM), fluorescence spectroscopy, and measurements of electrical passivation behavior in electrolyte solution. Significantly, we then show that our entire functionalization protocol can be translated from planar Si substrates to Si nanowire sensor devices that were fabricated using silicon-on-insulator (SOI) substrates. Thus, we report herein the first example of phosphonate monolayer synthesis and derivatization on a nanoscale device substrate. Finally, we also demonstrate that label-free detection of DNA/PNA hybridization can be accomplished using these silicon nanowire devices.

## RESULTS AND DISCUSSION

### Thin-Film Properties of OH-Terminated Organophosphonate Monolayer Coatings on Planar Si/SiO<sub>2</sub> Surfaces.

We investigated the properties of self-assembled monolayers (SAMs) formed from 11-hydroxyundecylphosphonic acids on the native oxide of planar, single crystalline silicon surfaces using contact angle measurements, ellipsometry, X-ray photoelectron spectroscopy (XPS), X-ray reflectivity, and atomic force microscopy (AFM).

**AFM.** Atomic force microscopy (AFM) analysis was done on a film of 11-hydroxyundecylphosphonate that was formed on the native SiO<sub>2</sub> termination of the Si substrate following two deposition steps (see Methods Section). AFM showed comprehensive surface coverage with a root-mean-square (rms) roughness of  $\sim 0.3$  nm, comparable to that of the supporting surface,  $\sim 0.2$  nm. This analysis could clearly distinguish between partial monolayer (island) formation, which was typically observed after a single deposition step, and a nearly complete monolayer, which was formed after two deposition steps (see Figure 2).

**Ellipsometry.** Ellipsometry measurements on seven independently coated samples indicated the average height of the organophosphonate thin film to be  $1.0 \pm 0.2$  nm after two depositions (estimated SiO<sub>2</sub> thickness  $\sim 2.1$  nm). This measured thickness of the organic adlayer is consistent with a monolayer whose alkyl chains are tilted by  $\sim 54^\circ$  with respect to the surface normal (estimated molecule length  $\sim 1.7$  nm). This value exceeds the previously reported tilt angle for compact monolayers of similar composition by about  $10^\circ$ ,<sup>12</sup> which may be explained by a slightly less complete layer in the present case. Local regions of reduced thickness may result in a thinner average thickness determined by ellipsometry thereby leading to a larger apparent tilt angle. Multipoint measurements performed at five locations on larger samples ( $3 \times 3$  cm<sup>2</sup>) indicated consistent formation of the monolayer on the scale of the ellipsometric resolution.

**Contact Angle.** The wetting behavior of the deposited phosphonate layer was determined by contact angle measurements. A value of  $(74 \pm 5)^\circ$  was recorded after two deposition steps, and is indicative of a moderately hydrophilic surface that is substantially absent of multilayers of the starting phosphonic acid. Smaller contact angles ( $\sim 50^\circ$ ) have been measured for compact,  $-\text{OH}$  terminated phosphonate monolayers;<sup>16</sup> thus we assign our finding to local regions of surface-exposed aliphatic groups, consistent with our larger measured tilt angle and, presumably, slightly less than 100% coverage of the surface. Minor distortions of the hydrogen-bonding network at the top of the hydroxylated film may easily lead to a significant increase in contact angle, in agreement with reports comparing dense and less densely packed hydroxyl-terminated monolayers.<sup>17</sup>

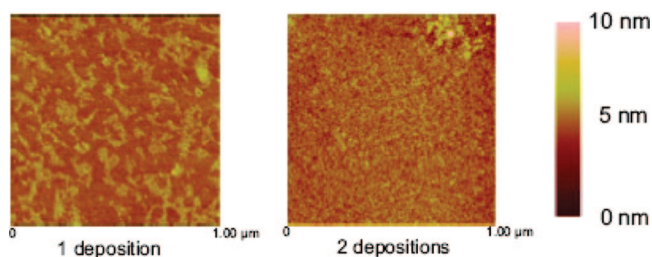


**Figure 2.** AFM pictures of an 11-hydroxyundecylphosphonate coating on Si/SiO<sub>2</sub>: (left) after one deposition step; (right) after two depositions. The region of higher topology in the right upper corner is assigned to residual multilayers.

**XPS.** The elemental composition of the surface was investigated by X-ray photoelectron spectroscopy (XPS). In particular, the phosphorus P2p doublet was detected at 134 eV ( $h\nu = 270$  eV), indicating the presence of the phosphonate on the surface (data not shown).

**X-ray Reflectivity.** X-ray reflectivity measurements were performed on a SAM of 11-hydroxyundecylphosphonate on SiO<sub>2</sub>/Si immersed into deionized water. The reflectivity curve (reflectivity,  $R$ , as a function of momentum transfer  $q$ , cf. Figure 3) exhibits the total reflection plateau ( $R = 1$ ) associated with the density difference of Si to water, and an intensity drop of several orders of magnitude. Details of the Si/SAM/water interface give rise to a broad peak at higher  $q$ . The analysis of these data was performed using the Parrat formalism.<sup>18</sup> A good fit of the data was possible as shown in Figure 3 (solid curve). To obtain this fit, the electron density depth profile of the interface was separated into the silicon substrate, the water reservoir, and the organic film. Bulk electron densities used were for Si,  $\rho_{\text{Si}} = 0.699$  e/Å<sup>3</sup>, and for water,  $\rho_{\text{H}_2\text{O}} = 0.334$  e/Å<sup>3</sup>. The density profile of the film was parametrized by a three box model. The density profile which

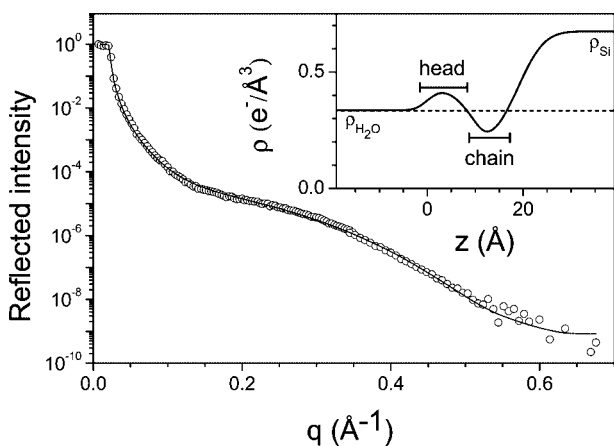


**Figure 3.** X-ray reflectivity. The reflected intensity is plotted as a function of the scattering vector  $q = (4\pi/\lambda) \sin(2\tau/2)$ . Here,  $\lambda$  is the X-ray wavelength and  $2\tau$  is the detector angle. The open circles are data; the solid curve is a best fit made according to a three-box model of the electron density profile. The inset shows the respective electron density profile. The dashed line indicates the bulk density of water. The two bars indicate regions of reduced and enhanced electron density, identified as “head” and “chain” regions.

resulted in the best fit of the data is inset as a solid curve in Figure 3. A reduced density region ( $\rho_{\text{chain}} = 0.25$  e/Å<sup>3</sup>) was observed adjacent to the Si substrate. This value is in good agreement with electron densities observed for hydrophobic regions, for example, in phospholipid membranes, that typically range from 0.23 to 0.30 e/Å<sup>3</sup>.<sup>19</sup> The presence of this region suggests the formation of a carbon-rich chain and a water-depleted region confined to the Si interface, with a thickness of about  $8 \pm 1$  Å (see the bar labeled “chain” in the inset of Figure 3). This thickness compares well with the length of the carbon chain part of C11–OH ( $\sim 13$  Å) if an average molecule tilt angle of 52° is assumed. This tilt angle is in excellent agreement with the average value determined by ellipsometry.

A region of enhanced electron density ( $\rho_{\text{head}} = 0.41$  e/Å<sup>3</sup>) with respect to the density of water is observed adjacent to the water reservoir. This suggests that coadsorption of, for example, Na ions occurs at the SAM-water interface. The integrated excess electron density (= excess charge per area) of this region is  $\rho_{\text{s,head}} - \rho_{\text{s,H}_2\text{O}} = 0.35$  e/Å<sup>2</sup>, which is equivalent to about one Na ion for every 31 Å<sup>2</sup>. Measurements at ambient conditions confirm the presence of this region of enhanced density.

**Functionalization with Heterobifunctional Linkers.** We investigated the conversion of the hydroxy-terminated monolayer to a maleimido-terminated monolayer using a series of bifunctional linkers.<sup>20</sup> Maleimido groups react with thiol functionality under mild conditions and thus have appealing properties for the immobilization of biomolecules such as DNA-oligonucleotides or proteins.<sup>21</sup> However, surface reactions are disadvantaged in that interfacial effects, such as steric hindrance, can prevent their going to completion. While hydroxyl-terminated SAMs can be more difficult to derivatize than amino- or carboxylic acid-terminated ones,<sup>22</sup> their use avoids nonspecific reactions among the terminal groups themselves (cross-linking) or reactions with the SiO<sub>2</sub> surface. Furthermore, chemical reactivity of the SAM is not the only parameter to be considered in the present study. The detection sensitivity of electrolyte gated field effect sensing devices is strongly dependent on the distance between the charged biomolecule to be detected and the semiconductor surface, which is due to the exponential decay of the electrical potential into electrolyte solution on the scale of the Debye screening length. In this context, the shortest available linker, 3-maleimidopropionic-acid-*N*-hydroxy-succinimidester (**1**), estimated length  $\approx 10$  Å, was chosen as a suitably reactive intermediate for the bioimmobilization step.

**XPS.** An N1s XPS spectrum of the monolayers obtained by coupling with linker **1** is shown in

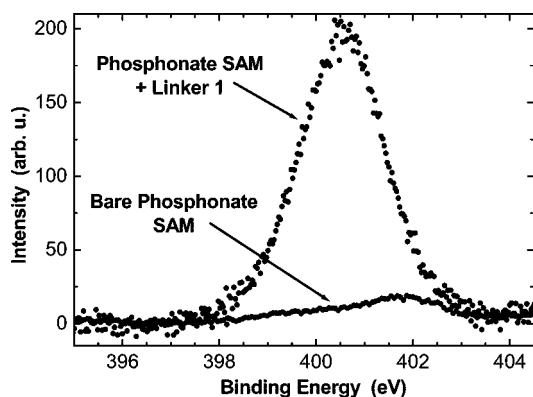


Figure 4. XPS spectra of the N1s region of 11-hydroxyundecylphosphonate monolayers modified with linker 1, compared to a reference sample without any linker functionalization.

Figure 4. Essentially no N1s signal was observed in a control experiment in which an 11-hydroxyundecylphosphonic acid SAM was treated under the same derivatization reaction conditions, but without the linker. On the basis of XPS analysis, the overall surface coverage for linker 1 was determined to be about 35%. We obtained this result by comparing areas of N1s main line spectra of our samples to those of saturated SAMs from CN-terminated alkylthiolates on gold, the coverage of which are known.<sup>23</sup> This estimate is in good agreement to a previously reported coupling yield of 40%, directly determined using gravimetric measurements (quartz crystal microbalance) for phosphonate layers on titanium dioxide on Ti.<sup>24</sup>

**Ellipsometry/Contact Angle.** Ellipsometry analysis indicated that the thickness of the surface layer increased by  $\sim 0.5$  nm for the maleimido coupling step, which is consistent with a surface immobilization yield of roughly 50%. Contact angles measured for water wetting were  $(72 \pm 5)^\circ$ , and hence did not change on derivatization within the measurement accuracy.

**PNA Immobilization.** Cysteine modified PNA-oligonucleotides (12 mer) were coupled to the maleimido activated surface<sup>25</sup> by standard Michael addition.

**XPS and Contact Angle Measurements.** AFM analysis and ellipsometry are not suitable to quantify the third synthetic step; thus we used XPS characterization to monitor the PNA immobilization, by following the nitrogen content of the treated samples.<sup>26</sup> As shown in Figure 5, the N1s XPS data showed a strong increase of the nitrogen content compared to the reference sample that contained only linker 1. Note that the large width of  $\sim 2.6$  eV of the N1s maximum obtained for the PNA layer, which certainly contains contributions from inhomogeneous broadening, excludes unambiguous determination of contributions from nitrogen in different chemical environments by fitting procedures.

Partial physical adsorption of the PNA onto the phosphonate monolayer *versus* complete, covalent im-

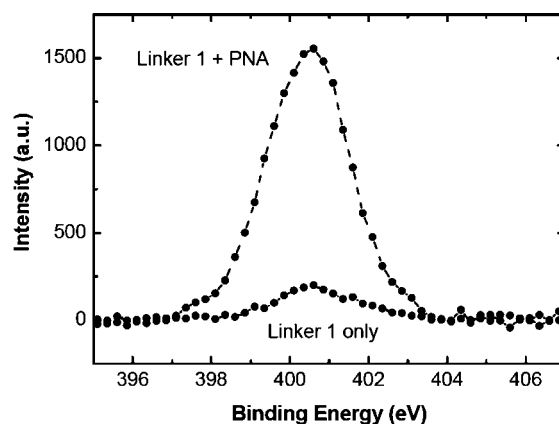


Figure 5. XPS spectra of the N1s region of 11-hydroxyundecylphosphonate monolayers modified with linker 1 and PNA, compared to a reference sample with linker 1 only.

mobilization could not be discerned from our characterization studies. However, quantitative analysis of N1s XPS spectra recorded after extensive washing, with sonication, showed no significant loss of the nitrogen content (data not shown), which indicates covalent linkage of the PNA to the monolayer. The PNA functionalized surface showed high stability under the electrochemical conditions of the sensing measurement: no significant degradation of the nitrogen signal was detected after prolonged immersion in standard aqueous buffer solutions, with substrate and solution held at electrical ground potential (data not shown).

Contact angle measurements showed an increased hydrophilic character of the surface, with contact angles  $(59 \pm 5)^\circ$ . This finding is in qualitative agreement with the expectation for PNA due to its polar structural groups.

**Hybridization: Fluorescence, Contact Angle.** We carried out fluorescence measurements of dye-labeled DNA oligonucleotides on planar, PNA functionalized samples before DNA sensing experiments using SiNW devices in order to verify the hybridization reaction. Different regions of the same PNA-functionalized sample were exposed to complementary and noncomplementary DNA oligonucleotides, both labeled with the same fluorophore (Cy3), and the corresponding fluorescence spectra were subsequently recorded. A significant increase in intensity, by about a factor of five, was measured at the peak wavelength for Cy3 fluorescence for the regions treated with cDNA as compared to the regions treated with noncDNA (data not shown). Contact angle measurements on regions treated with cDNA indicated a further increased hydrophilic character  $(44 \pm 5)^\circ$  compared to the unconjugated PNA-coated sample, in agreement with the expectation for increasing the content of hydrophilic molecules (DNA) on the surface. In regions exposed to noncDNA the contact angle  $(53 \pm 5)^\circ$  did not significantly change.

**Label-free Detection of DNA/PNA Hybridization.** Having successfully accomplished the specific immobilization of

PNA onto planar, SiO<sub>2</sub>-covered Si surfaces we translated the complete functionalization protocol to silicon nanowire (SiNW) devices to investigate the electronic, label-free detection of DNA/PNA hybridization.

#### Silicon Nanowire Fabrication.

SiNW sensors were fabricated using p-doped silicon-on-insulator (SOI) wafers by a combination of electron beam lithography (EBL) and subsequent reactive ion etching (RIE). Typically, one sensor device consisted of a set of one to five NWs measured in parallel. Figure 6 shows a schematic sketch of one single SiNW sensor chip and a scanning electron micrograph (SEM) of five 2 μm long, ~100 nm wide SiNWs.

**Electrochemical Passivation.** An absolute requirement for electrolyte-gated operation of a SiNW sensor device is that any electrochemical leakage current across the silicon/electrolyte interface must be minimized in the voltage range of the sensing experiment. To probe the passivating behavior of the phosphonate monolayer coating, we varied the potential of a phosphonate functionalized SiNW with respect to a Ag/AgCl reference electrode, and recorded the resulting current (Figure 7). Only negligibly small current amplitudes, of the order of 10 pA, were observed between -0.2 and 0.2 V. Thus, the phosphonate layer provided excellent passivation under the conditions of the sensing experiment in which the electrolyte potential was set to the potential of the substrate (= 0 V in Figure 7). After removal of the monolayer using an oxygen plasma we recorded a strong increase in the current, in particular for the negative voltage range, which can be assigned to reduction of H<sup>+</sup> to hydrogen at the substrate surface.<sup>27</sup>

**Electronic Detection of DNA Using PNA-Functionalized SiNW Devices.** For the electrical detection of DNA/PNA hybridization, a sensor chip functionalized with single-stranded 12 mer PNA was built into a fluidic chamber, and its resistance was recorded as a function of time while the SiNWs were exposed to buffer solutions of different composition. Typically, the resistance of one nanowire was of the order of 50 kΩ. Resistance changes upon hybridization however could be anticipated to be of the order of 10 Ω only, for a realistic surface potential change of a few mV upon DNA hybridization,<sup>9</sup> and taking into account the  $\Delta R(\Delta V_{\text{Ag/AgCl}})$  calibration carried out prior to the experiment (see Methods Section, and ref 28). To achieve a sufficiently large signal-to-noise ratio we used a phase-sensitive, low-noise amplifier electrical measurement setup (see Methods Section). In addition to the small changes in resistance that had to be resolved, the devices generally exhibited

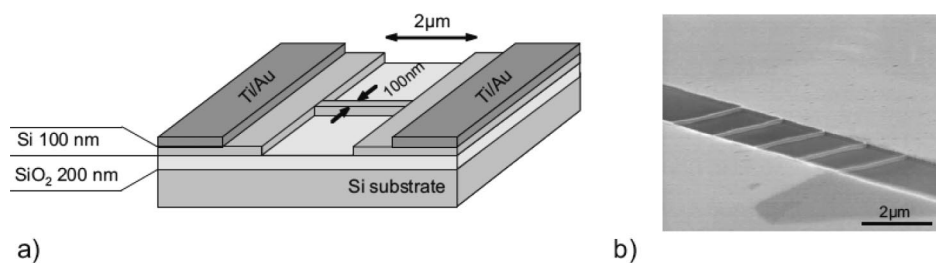


Figure 6. (a) Schematic of a single silicon nanowire (SiNW) sensing device. The processed silicon-on-insulator (SOI) substrate consists of, from top to bottom: Ti/Au (20 nm/200 nm) contact pads; top silicon layer (100 nm, p-doped  $10^{18} \text{ cm}^{-3}$ ); light gray: buried SiO<sub>2</sub> (200 nm); Si handle wafer (approximately 500 μm). (b) SEM micrograph showing a set of five 2 μm long, 100 nm wide (and high), parallel SiNWs. The SiNWs were fabricated by electron beam lithography (EBL) and subsequent reactive ion etching (RIE).

drift on time scales of the order of 10 minutes after solution exchange. This drift may possibly be assigned to ions penetrating into the phosphonate monolayer eventually inducing slow chemical modification of the oxide surface as a result of partial exposure to these ions.<sup>29</sup> Once an equilibrium resistance signal was attained, the buffer was exchanged by pumping solution through the fluidic chamber system. After pumping, the fluid was again allowed to rest before taking the next resistance value after equilibrating. Data from a typical hybridization experiment that consisted of three sequential solution exchange steps is shown in Figure 8. First, the chip was maintained in a buffered saline of low ionic strength (step 1). Then, 1 μM cDNA dissolved in the same buffered saline was introduced for 25 min (step 2); finally, this medium was exchanged for the pure electrolyte solution of step 1 (step 3). As shown in Figure 8, we observed a distinct decrease in resistance upon injecting the solution containing cDNA. We attribute this decrease to an increase in negative surface charge on hybridization, essentially by the surface adsorbing DNA. This additional negative charge of DNA leads to an accumulation of charge carriers (holes) close to the surface inside the p-doped silicon nanowire, thereby lowering its resistance. Taking into account the  $\Delta R(\Delta V_{\text{Ag/AgCl}})$  calibration, this measured change in resistance corresponds to a change in sur-

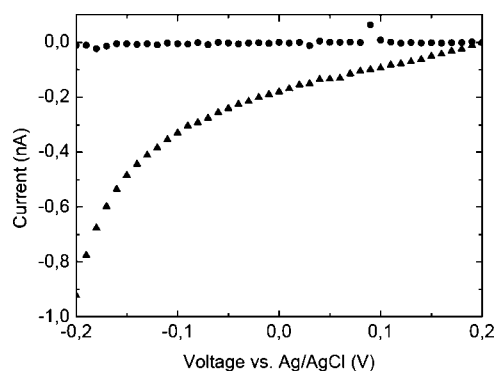
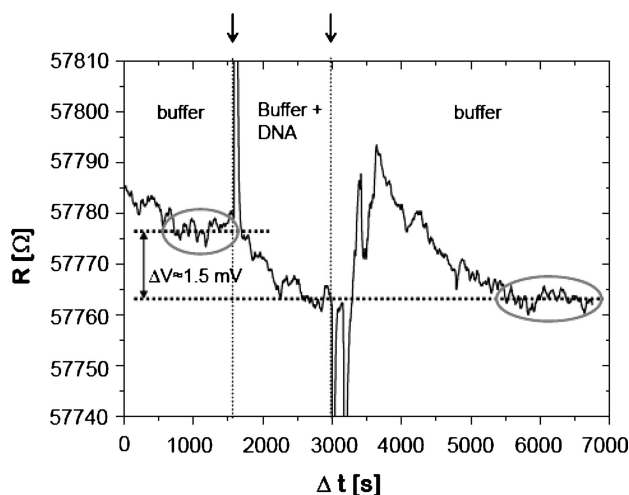


Figure 7. Leakage current measured between the drain contact of the SiNW FET and the Ag/AgCl electrolyte reference electrode, as a function of drain potential, for a phosphonate layer-passivated device (●) and after treatment in O<sub>2</sub> plasma (monolayer removed) (▲).



**Figure 8.** Hybridization experiment: Resistance of a 12 mer PNA-functionalized single nanowire as a function of time. Starting with pure buffer solution (reference signal level), the left arrow/dashed vertical line indicates injection of buffer containing a  $1 \mu\text{M}$  solution of complementary 12 mer DNA. The right arrow/line indicates solution replacement with pure buffer solution. Grey ovals mark two stable regions whose difference in resistance corresponds to a change in surface potential of  $\Delta V \approx 1.5 \text{ mV}$ , as indicated. Strong transient resistance changes at the beginning of each interval derive from solution pumping through the fluidic chamber.

face potential of  $\sim 1.5 \text{ mV}$ . We routinely obtained values of the order of a few mV in several independent experiments, which conform well to magnitudes reported in the literature.<sup>9</sup> It should be mentioned, however, that in some experimental runs a signal of nearly comparable magnitude was observed for mismatched DNA. Thus, in contrast to fluorescence measurements, this finding suggests that nonspecific adsorption of DNA onto the organophosphonate monolayer may be significant in label-free sensing experiments. We are currently investigating modification of the organic interfacial layer to effectively reduce these nonspecific interactions.

## CONCLUSIONS

We investigated hydroxyalkylphosphonate self-assembled monolayers as interface systems for the

## METHODS SECTION

**Materials and Cleaning.** All chemicals were purchased from Sigma-Aldrich unless otherwise indicated. Oligo-DNA, 5'-labeled with fluorophore Cy3 was purchased from IBA, Göttingen; modified oligo-PNA was obtained from Eurogentec, Cologne. 11-Hydroxyundecyl phosphonic acid was synthesized as previously reported.<sup>31</sup> Substrates used for characterization on planar surfaces were 4-in. Si (100) wafers, p-doped (boron),  $0.005\text{--}0.018 \text{ Ohm}\cdot\text{cm}$ , from Wacker, Burghausen, Germany. Samples ( $1 \times 1 \text{ cm}^2$ ) were cut from these wafers and cleaned in acetone with sonication for 10 min, followed by extensive rinsing in isopropyl alcohol and water. The samples were further washed in a solution of water/ $\text{H}_2\text{O}_2$  30%/NH<sub>4</sub>OH 5:1:1 at  $80 \text{ }^\circ\text{C}$  for 10 min, followed by extensive rinsing with sonication in water for 10 min. The samples were blown dry with nitrogen, cleaned in an oxy-

PNA-functionalization of silicon nanowire sensor devices for label-free biosensing applications. AFM and ellipsometric analysis on planar silicon surfaces indicated the presence of an almost complete, dense monolayer on the native oxide with thickness ca. 1 nm. This monolayer comprises alkylphosphonate molecules that are, on average, tilted by about  $54^\circ$  from the surface normal. This finding was further confirmed by X-ray reflection measurements done in aqueous solution, which revealed a dense hydrophobic region of about  $8 \text{ \AA}$  thickness (corresponding to a tilt angle  $52^\circ$ ) that was separated from an additional layer of enhanced density suggesting coadsorption of ions on top of the SAM. The monolayer effectively passivates the Si surface against electrochemical leakage current into the electrolyte solution through the interface, with maximum currents of the order of 10 pA measured at 200 mV. Functionalization of the phosphonate monolayer with a heterobifunctional maleimido compound was mainly verified by N1s XPS, which indicated a yield of about 35%. The subsequent functionalization with PNA oligonucleotides was verified by XPS, contact angle measurements, and fluorescence spectroscopy following hybridization with dye-labeled DNA. This protocol was translated to 100 nm wide p-doped Si nanowire field-effect devices fabricated from SOI, thereby constituting the first successful example of phosphonate monolayer synthesis and derivatization on a silicon-based, nanoelectronic device. The PNA-functionalized nanowire devices allowed for label-free detection of DNA hybridization. A decrease in wire resistance equivalent to a surface potential change of  $\sim 1.5 \text{ mV}$  was measured upon injection of  $1 \mu\text{M}$  DNA electrolyte buffer solution. This result is in agreement with the expectation for hybridization that results in the surface adsorbing negative charges from the DNA. Future work will focus on reduction of nonspecific DNA adsorption effects and monolithic integration of these sensor structures into microfluidic systems.<sup>30</sup>

gen plasma (200 W, 5 min), and then immediately used for the preparation of the phosphonate monolayers.

**Formation of Self-Assembled Monolayers.** 11-Hydroxyundecylphosphonic acid formed self-assembled monolayers (SAMs) on the clean native SiO<sub>2</sub> terminating a single crystal silicon surface by holding the sample pieces vertically in a  $25 \mu\text{M}$  solution of the acid dissolved in dry THF; the solvent was allowed to evaporate slowly such that the meniscus traversed the surface of the sample, thereby transferring the phosphonic acid to the SiO<sub>2</sub>/Si. The solution reservoir was kept large enough such that there was no appreciable change in the concentration of the phosphonic acid during this process. Coated samples were then gently removed from their holders and put into an oven at  $120 \text{ }^\circ\text{C}$  for 18–20 h to convert the hydrogen bonded phosphonic acid monolayer to the covalently bonded phosphonate one. Hydrogen bonding among phosphonate head-groups and hydroxyl

tail groups of the starting 11-hydroxyundecylphosphonic acid can give rise to surface multilayers. For this reason, all samples were carefully washed twice with sonication in methanol for 10 min followed by washing with sonication in a solution of water/THF/triethylamine 10:3:1 for 5 min, and a further wash for 10 min in water with sonication. Samples were dried under a nitrogen flux. To obtain complete coverage of the silicon surface a second functionalization process was usually performed by repeating the above deposition steps. A third layer deposition usually did not further improve the quality of the monolayers, so only two surface treatments were routinely performed.

**Bonding 1 to the Phosphonate Monolayer.** Si/SiO<sub>2</sub> samples coated with the 11-hydroxyundecylphosphonate monolayer were kept overnight in a stirred 19 mM solution of 3-maleimidopropionic acid-NHS (**1**) in dry acetonitrile at room temperature under argon and then rinsed with acetonitrile with sonication for 5 min and then with THF with sonication for 5–10 min. All operations were carried out under argon. Samples were typically dried under nitrogen flux, stored under vacuum, and washed briefly with water just prior to the coupling reaction with PNA.

**Immobilization of PNA Oligonucleotides.** PNA-oligonucleotides (12 mer) (5'-Cys-TAGTCGGAAGCA-Lys-3') were dissolved in degassed water (pH 7.0) and diluted to a concentration of 25 μM. Small drops of the solution were deposited manually on the surface of the sample chips that had been prepared with the organophosphonate monolayer and freshly treated with **1**. The chips were incubated overnight at room temperature in a humidified chamber to prevent the drying and were then washed carefully with sonication in water (5 to 10 min); they were finally blown dry with nitrogen.

**Hybridization Conditions.** Complementary 12 mer DNA-oligonucleotides (5'-TGCTCCGACTA-3') were diluted in a hybridization buffer consisting of 2 mM 3-morpholinopropanesulfonic acid (MOPS)<sup>32</sup> and 3 mM NaCl, to a final concentration of 1 μM at pH 6.8. As the noncDNA sequence 5'-ACTAATCTTAT-3' was used. For fluorescence measurements, the oligonucleotides were dye labeled (Cy3) at their 5' end. The chips were incubated in the hybridization solution for 25 min at room temperature, then washed carefully three times with buffer solution, then with water (without sonication), and blown dry under nitrogen.

**Contact Angle Measurements.** Contact angle measurements were made using a OCA 15 plus instrument (DataPhysics, Stuttgart) on 1–2 samples per functionalization, and 3 × 2 (left/right) angles per sample were taken at different locations on each surface: A drop of water was deposited using a microsyringe, and the wetting angle was recorded immediately. Standard deviations were between 1° and 5° for all samples whereby the latter value was taken as estimated maximum error bar (±5°) for all measured mean values.

**Characterization by XPS.** Low-resolution XPS data were obtained using nonmonochromatized Al and Mg K $\alpha$  radiation and a hemispherical electron energy analyzer (100 mm radius). The analyzer was equipped with a position sensitive resistive anode detector for increased sensitivity. High-resolution XPS data were recorded at the U49-II-PGM-1 beamline of the synchrotron radiation source BESSY, Berlin, using a hemispherical electron energy analyzer equipped with five channeltrons. By suitable choice of incident irradiation, the P2p<sub>3/2,1/2</sub> emission could be well separated from Si plasmon features. For these high-resolution measurements, the overall energy resolution ( $\Delta h\nu$  and  $\Delta E_k$ ) was set to 0.4 eV.

**Thickness Measurements by Ellipsometry.** Ellipsometric measurements were performed using an EL X-02C rotating-analyzer-ellipsometer (DRE Dr. Riss, Ratzeburg) equipped with a HeNe laser ( $\lambda = 632.8$  nm) at an angle of incidence of 70°. Layer thicknesses were obtained by averaging five measurement points for each sample. A refractive index value of  $n = 1.46$  was used for the organic layer<sup>33</sup> for the thickness calculation.

**Fluorescence Detection.** Fluorescence measurements were made by positioning a custom-made optical fiber mount over the chip. Green light from an Ar<sup>+</sup> laser ( $\lambda = 514$  nm) was guided onto the surface at an angle of approximately 45°, and light emitted from the sample was collected by a second fiber oriented normal to the surface plane. This light was coupled from the detec-

tion fiber into a grating monochromator equipped with a cooled photomultiplier operating in single-photon-counting mode, for spectral analysis.

**X-Ray Reflectivity.** Details of the sample chamber and measurement technique have been described elsewhere.<sup>34</sup> Briefly, the functionalized Si wafer piece was embedded into a microfluidic chamber, and an X-ray energy of 19.49 keV was used to minimize intensity losses due to absorption. Experiments reported here have been performed at ID1 at the European Synchrotron Radiation Facility (ESRF).

**Atomic Force Microscopy.** A Nanoscope IIIa from Digital Instruments was used for the experiments. Data were acquired in tapping mode.

**Silicon Nanowire Device Fabrication.** Silicon nanowire (SiNW) sensors were fabricated using silicon-on-insulator (SOI) wafers (ELTRAN, Canon). The SOI wafers consisted of a top silicon layer (thickness 100 nm, boron p-doped 10<sup>18</sup> cm<sup>-3</sup> by ion-implantation, Fraunhofer Institute, Freiburg), separated from the bulk silicon substrate by a buried silicon dioxide layer (thickness 200 nm). Ohmic contacts (Ti/Au 20/200 nm) were deposited on the top silicon layer by standard optical lithography and metal evaporation techniques. Silicon nanowires (NWs) including micrometer-scale electrical leads were patterned from the top silicon layer by a combination of electron beam lithography (EBL) and subsequent reactive ion etching (RIE) using a combination of SF<sub>6</sub> and C<sub>4</sub>F<sub>8</sub> as reactive etch gases. Typically, one sensor device consisted of a set of one to five NWs measured in parallel.

**SiNW Functionalization.** After the fabrication of the SiNWs the devices were cleaned and biofunctionalized with single stranded 12 mer PNA probe molecules as described above. No special care was taken to mechanically protect the oxide supported SiNWs.

**Electrical Setup.** For electrical measurements the sensor device chip was built into a custom-made fluidic chamber with liquid access to the central NW region only, thereby excluding the metallic contacts outside. An alternating voltage (internal oscillator of lock-in amplifier,  $V_{rms}$  amplitude 0.2 mV,  $f = 11$  Hz) was applied between source and drain of the device in a standard lock-in conductance measurement setup. The resulting current was preamplified using a DL Instruments LLC 1211 amplifier, and the proportional output voltage was then measured with an EG&G PAR 124A lock-in amplifier having an integrated differential preamplifier. A Ag/AgCl reference electrode accessing the fluid volume above the sensing chip allowed for a variation of the electrolyte potential vs source potential. In this way, the change of NW resistance as a function of surface potential variation could be calibrated.<sup>28</sup> Strictly, both, the silicon nanowires and their micrometer-scale silicon leads contribute to the measured change in resistance. From a comparison to reference measurements however, on directly contacted leads (no nanowire patterned in-between), we estimate that for a single wire experiment the observed changes in resistance may be assigned to about 95% to originate from the wire, and only to about 5% from the leads. For this reason we neglected the lead contribution in the discussion of the PNA-DNA hybridization experiments. During the hybridization experiments the electrolyte potential was always set to ground. Routinely, before functionalizing the SiNWs their electrical properties were tested under dry conditions by measuring their current–voltage characteristics. Only sensor devices exhibiting Ohmic characteristics were chosen for further investigation. DNA hybridization studies were carried out by monitoring the conductance of the SiNWs over time while electrolyte buffer containing DNA was flushed through the fluidic chamber. An electrolyte buffered saline solution of low ionic strength (2 mM MOPS, 3 mM NaCl, pH 6.8, ionic strength = 4.3 mM) was used.

Measurements of the electrochemical leakage current across the silicon/electrolyte interface were performed by sweeping the DC potential of a phosphonate functionalized SiNW with respect to a Ag/AgCl reference electrode at a rate of 26 mV/min, and recording the resulting current, using a Keithley 2400 source meter. The average from 10 current values was taken at each bias voltage.

**Acknowledgment.** We are grateful to K. Buchholz and A. Solovov for their earlier contributions and thank K. Arinaga, S. Birner, F. Blobner, D. Dorfner, A.G. Hansen, E.L. Hanson, U. Rant, and S. Strobel for helpful discussions and experimental support. This work was financially supported by the DFG via SFB563 and the Nanosystems Initiative Munich, and by the Fujitsu Laboratories of Europe. M.T. gratefully acknowledges funding by the BMBF (Junior Research Group "Nanotechnology", grants 03N8713 and 03X5513). J.S. and M.D. thank the National Science Foundation for support of their research (CHE-0612572).

## REFERENCES AND NOTES

- Fritz, J.; Cooper, E. B.; Gaudet, S.; Sorger, P. K.; Manalis, S. R. Electronic Detection of DNA by its Intrinsic Molecular Charge. *Proc. Natl. Acad. Sci. U.S.A.* **2002**, *99*, 14142–14146.
- Ingebrandt, S.; Offenhausser, A. Label-Free Detection of DNA Using Field-Effect Transistors. *Phys. Status Solidi A* **2006**, *203*, 3399–3411.
- Uno, T.; Tabata, H.; Kawai, T. Peptide-Nucleic Acid-Modified Ion-Sensitive Field-Effect Transistor-Based Biosensor for Direct Detection of DNA Hybridization. *Anal. Chem.* **2007**, *79*, 52–59.
- Pouthas, F.; Gentil, C.; Cote, D.; Bockelmann, U. DNA Detection on Transistor Arrays Following Mutation-Specific Enzymatic Amplification. *Appl. Phys. Lett.* **2004**, *84*, 1594–1596.
- Hahn, J.; Lieber, C. M. Direct Ultrasensitive Electrical Detection of DNA and DNA Sequence Variations Using Nanowire Nanosensors. *Nano Lett.* **2004**, *4*, 51–54.
- Li, Z.; Rajendran, B.; Kamins, T. I.; Li, X.; Chen, Y.; Williams, R. S. Silicon Nanowires for Sequence-Specific DNA Sensing: Device Fabrication and Simulation. *Appl. Phys. A* **2005**, *80*, 1257–1263.
- Gao, Z. Q.; Agarwal, A.; Trigg, A. D.; Singh, N.; Fang, C.; Tung, C. H.; Fan, Y.; Buddharaju, K. D.; Kong, J. M. Silicon Nanowire Arrays for Label-Free Detection of DNA. *Anal. Chem.* **2007**, *79*, 3291–3297.
- Stutzmann, M.; Garrido, J. A.; Eickhoff, M.; Brandt, M. S. Direct Biofunctionalization of Semiconductors: A Survey. *Phys. Status Solidi A* **2006**, *203*, 3424–3437.
- Poghossian, A.; Cherstvy, A.; Ingebrandt, S.; Offenhausser, A.; Schöning, M. J. Possibilities and Limitations of Label-Free Detection of DNA Hybridization with Field-Effect-Based Devices. *Sens. Actuators, B* **2005**, *111*, 470–480.
- Bard, A. J.; Faulkner, L. R. *Electrochemical Methods—Fundamentals and Applications*, 2nd ed.; John Wiley & Sons: New York, 2000.
- Silverman, B. M.; Wieghaus, K. A.; Schwartz, J. Comparative Properties of Siloxane vs Phosphonate Monolayers on a Key Titanium Alloy. *Langmuir* **2005**, *21*, 225–228.
- Hanson, E. L.; Schwartz, J.; Nickel, B.; Koch, N.; Danisman, M. F. Bonding Self-Assembled, Compact Organophosphonate Monolayers to the Native Oxide Surface of Silicon. *J. Am. Chem. Soc.* **2003**, *125*, 16074–16080.
- Nielsen, P. E.; Haaima, G. Peptide Nucleic Acid (PNA). A DNA Mimic with a Pseudopeptide Backbone. *Chem. Soc. Rev.* **1997**, *26*, 73–78.
- Jensen, K. K.; Orum, H.; Nielsen, P. E.; Norden, B. Kinetics for Hybridization of Peptide Nucleic Acids (PNA) with DNA and RNA Studied with the BIACore Technique. *Biochemistry* **1997**, *36*, 5072–5077.
- Manning, G. S. The Molecular Theory of Polyelectrolyte Solutions with Applications to the Electrostatic Properties of Polynucleotides. *Q. Rev. Biophys.* **1978**, *2*, 179–246.
- Hanson, E. L. Private communication, 2007.
- Berron, B.; Jennings, G. K. Loosely Packed Hydroxyl-Terminated SAMs on Gold. *Langmuir* **2006**, *22*, 7235–7240.
- Parrat, L. G. Surface Studies of Solids by Total Reflection of X-Rays. *Phys. Rev. B* **1954**, *95*, 359.
- Hochrein, M. B.; Reich, C.; Krause, B.; Radler, J. O.; Nickel, B. Structure and Mobility of Lipid Membranes on a Thermoplastic Substrate. *Langmuir* **2006**, *22*, 538–545.
- Sullivan, T. P.; Huck, W. T. S. Reactions on Monolayers: Organic Synthesis in Two Dimensions. *Eur. J. Org. Chem.* **2003**, *1*, 17–29.
- Wang, Y. Y.; Cai, J.; Rauscher, H.; Belun, R. H.; Goedel, W. A. Maleimido-Terminated Self-Assembled Monolayers. *Chem.—Eur. J.* **2005**, *11*, 3968–3978.
- Li, X. M.; Huskens, J.; Reinhoudt, D. N. Reactive Self-Assembled Monolayers on Flat and Nanoparticle Surfaces, and their Application in Soft and Scanning Probe Lithographic Nanofabrication Technologies. *J. Mater. Chem.* **2004**, *14*, 2954–2971.
- Frey, S.; Shaporenko, A.; Zharnikov, M.; Harder, P.; Allara, D. L. Self-Assembled Monolayers of Nitrile-Functionalized Alkanethiols on Gold and Silver Substrates. *J. Phys. Chem. B* **2003**, *107*, 7716–7725.
- Gawalt, E. S.; Avaltroni, M. J.; Danahy, M. P.; Silverman, B. M.; Hanson, E. L.; Midwood, K. S.; Schwarzbauer, J. E.; Schwartz, J. Bonding Organics to Ti Alloys: Facilitating Human Osteoblast Attachment and Spreading on Surgical Implant Materials. *Langmuir* **2003**, *19*, 200–204.
- Wang, Y. Y.; Prokein, T.; Hinz, M.; Seliger, H.; Goedel, W. A. Immobilization and Hybridization of Oligonucleotides on Maleimido-Terminated Self-Assembled Monolayers. *Anal. Biochem.* **2005**, *344*, 216–223.
- Petrovykh, D. Y.; Kimura-Suda, H.; Whitman, L. J.; Tarlov, M. J. Quantitative Analysis and Characterization of DNA Immobilized on Gold. *J. Am. Chem. Soc.* **2003**, *125*, 5219–5226.
- Lehmann, V. *Electrochemistry of Silicon*; Wiley-VCH: Weinheim, Germany, 2002.
- Nikolaides, M. G.; Rauschenbach, S.; Lubber, S.; Buchholz, K.; Tornow, M.; Abstreiter, G.; Bausch, A. R. Silicon-on-Insulator Based Thin-Film Resistor for Chemical and Biological Sensor Applications. *Chemphyschem* **2003**, *4*, 1104–1106.
- Jamasb, S.; Collins, S.; Smith, R. L. A Physical Model for Drift in pH ISFETs. *Sens. Actuators, B* **1998**, *49*, 146–155.
- Sharma, S.; Buchholz, K.; Lubber, S. M.; Rant, U.; Tornow, M.; Abstreiter, G. Silicon-on-Insulator Microfluidic Device with Monolithic Sensor Integration for Mu-TAS Applications. *IEEE J. Microelectromech. Syst.* **2006**, *15*, 308–313.
- Putvinski, T. M.; Schilling, M. L.; Katz, H. E.; Chidsey, C. E. D.; Mulsce, A. M.; Emerson, A. B. Self-Assembly of Organic Multilayers with Polar Order Using Zirconium-Phosphate Bonding between Layers. *Langmuir* **1990**, *6*, 1567–1571.
- Easterby, R. B. J. *Buffer Solutions: The Basics*; Oxford University Press: Oxford, U.K., 1996.
- Bain, C. D.; Troughton, E. B.; Tao, Y. T.; Evall, J.; Whitesides, G. M.; Nuzzo, R. G. Formation of Monolayer Films by the Spontaneous Assembly of Organic Thiols from Solution onto Gold. *J. Am. Chem. Soc.* **1989**, *111*, 321–335.
- Reich, C.; Hochrein, M. B.; Krause, B.; Nickel, B. A Microfluidic Setup for Studies of Solid-Liquid Interfaces Using X-Ray Reflectivity and Fluorescence Microscopy. *Rev. Sci. Instrum.* **2005**, *76*, 095103.